

Neutron studies of gauge field and charge in Ih heavy-water ice

D. J. P. Morris,^{1,*} K. Siemensmeyer,² J.-U. Hoffmann,² B. Klemke,² I. Glavatskyi,³ K. Seiffert,⁴
D. A. Tennant,⁵ S. V. Isakov,⁶ S. L. Sondhi,⁷ and R. Moessner⁸

¹*Department of Physics, Xavier University, 3800 Victory Parkway, Cincinnati, Ohio 45207, USA*

²*Helmholtz-Zentrum Berlin, Hahn-Meitner Platz 1, Berlin, Germany*

³*Scienion AG, Volmerstrasse 7b, 12489 Berlin, Germany*

⁴*Institut für Werkzeugmaschinen, Technische Universität Berlin, Pascalstrasse 8-9, 10587 Berlin, Germany*

⁵*Oak Ridge National Laboratory, P.O. Box 2008, MS-6477, Oak Ridge, Tennessee 37831, USA*

⁶*Google Inc., Brandschenkestrasse 110, 8002 Zurich, Switzerland*

⁷*Department of Physics, Princeton University, Washington Road, Princeton, New Jersey 08544, USA*

⁸*Max-Planck-Institut für Physik komplexer Systeme, Nothnitzer Strasse 38, 01187 Dresden, Germany*



(Received 24 January 2019; revised manuscript received 19 March 2019; published 20 May 2019)

The distinctive character of water ice results from the partially disordered combination of covalent and hydrogen bonds in the network of hydrogen and oxygen atoms. The nontrivial hydrogen correlations we report in diffuse neutron scattering are analytically fit via a description of this state as a topological system exhibiting an emergent gauge field. This allows for the density of correlation-terminating point defects to be determined as one defect per 500 oxygen sites at 30 K. Application of an analytical model of ice paves the way towards a detailed understanding of this ubiquitous solid.

DOI: [10.1103/PhysRevB.99.174111](https://doi.org/10.1103/PhysRevB.99.174111)

I. INTRODUCTION

Water ice (H₂O) is a unique solid whose structure and dynamics continue to excite interest. The special connectivity of the H^O_H polar molecules through the making and breaking of hydrogen bonds forms a dynamic network which can reconfigure to transport charge [1] while being of importance in a truly interdisciplinary range of fields from food science to biology [2]. In its common form, ice is made up of H₂O molecules within a hcp unit cell [Fig. 1(a)], referred to as the Ih phase, well known in everyday life. The oxygen atoms form a regular lattice, and each oxygen is surrounded by four hydrogen ions (protons, H⁺), each located on a line connecting the four nearest-neighbor oxygen sites [Fig. 1(b)]. The hydrogens are displaced from the midpoints between two oxygens, and each oxygen has two close hydrogens, keeping the H₂O molecular character. These structural constraints are encoded by the Bernal-Fowler ice rules [4], implying the residual ground-state entropy [5] of $R \ln \frac{3}{2}$ and the commonly accepted picture of hydrogen disorder: in the ground state, H₂O molecules form a quasidegenerate correlated network where the orientation of one molecule affects the orientation of adjacent molecules, which in turn affects the orientation of further molecules, propagating throughout the crystal. Previous diffuse elastic x-ray and neutron scattering studies of ice confirmed the ice rules using simulations in which molecules were orientated along random walks restricted by the ice rules [6–8] but lacked a description of the mechanism that led to the structure.

Work to combine ideas from topology and field theory along with a simple mapping of hydrogen displacement vectors onto pseudospins [9–15] has culminated in the development of a theoretical approach by Isakov *et al.* [3] and Benton *et al.* [16]. We present a diffuse neutron scattering experiment that tests this topological description of the structure of water ice at 30 K. While the scattering intensity of Bragg peaks reveals the long-range average occupation of crystallographic sites, diffuse scattering probes structural correlations of materials over a large spatial range from small displacement to long-range correlations. Diffuse scattering data covering a three-dimensional (3D) volume of reciprocal space provide a large data set to robustly test the theoretical predictions on the nano- to mesoscale structure.

The key idea of the topological order approach [3,16] is that the displacement vector from the oxygen bond midpoint to the occupied hydrogen site [Fig. 1(c)] is modeled as an Ising pseudospin \vec{s}_i [13]. The locations of the occupied hydrogen sites are given by $\vec{r}_{i\alpha} = \vec{r}_{i\alpha}^0 + d\vec{s}_{i\alpha}$, where $\vec{r}_{i\alpha}^0$ is the location of the midpoint between nearest-neighbor oxygen-oxygen, $d = 0.134R_{OO}$ is the length of the hydrogen displacement away from the center of the bond, and R_{OO} is the neighboring oxygen-oxygen distance, 2.76 Å. The pseudospins $\vec{s}_{i\alpha} = \pm 1$ indicate a nearby or faraway hydrogen for the hydrogen ion labeled α in the i th unit cell and should not be confused with any quantum-mechanical spin in the system. In fact, the pseudospin is a manifestation of an emergent gauge field, labeled \vec{B} , aligned with the pseudospins (Fig. 1(c); Ref. [9]). In a ground state, the total number of vectors pointing into each oxygen is equal to the number pointing out; therefore, the ice rules imply the averaged field is divergence free, $\nabla \cdot \vec{B} = 0$, as in conventional magnetostatics. A review of systems exhibiting emergent electromagnetic states is given

*morrisd3@xavier.edu

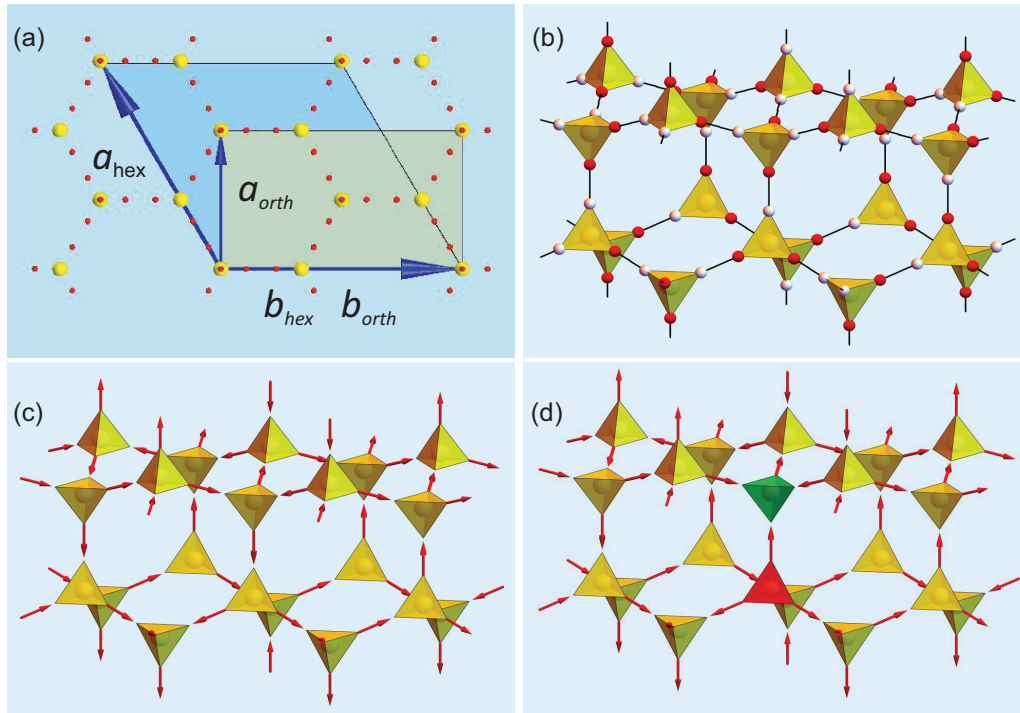


FIG. 1. The Coulomb liquid structure of water ice. (a) The Ih phase of water ice is made up of hexagonal unit cells ($\vec{a}_{\text{hex}}, \vec{b}_{\text{hex}}$), although an equally justifiable unit cell is the smaller orthogonal unit cell used in this study ($\vec{a}_{\text{orth}}, \vec{b}_{\text{orth}}$), shown here with yellow oxygen and red hydrogen sites. (b) The water molecules in the common form of ice (Ih) are arranged as connected tetrahedra obeying the ice rules. The oxygen sits at the center of the tetrahedron, surrounded by four protons which can occupy one of two possible sites shown in red (vacant) and white (occupied) between any pair of neighboring oxygens. (c) The displacement of the occupied hydrogen site away from the O-O midpoint is modeled as a pseudospin [3]. (d) Point defects terminate the hydrogen correlations and break the ice rules locally; for example, net plus (H_3O^+ , green) and minus charges (OH^- , pink) can form, separate via pseudospin flips, and carry electric current.

in Ref. [17], and one on topology and (spin) ice physics is given in Ref. [18].

II. EXPERIMENT

A. Sample preparation

Heavy-water ice (D_2O) samples were used that contained the deuterium isotope, instead of hydrogen, as it provides a less incoherent background in neutron scattering [19]. High-quality single crystals of D_2O were grown with a modified Bridgeman technique based on work by Ohtomo *et al.* [20] in which a temperature gradient slowly moves along a sample growth cell containing liquid D_2O .

The crystal growth apparatus was constructed from a cold-liquid bath (23% ethylene glycol:water solution) cooled by a Julbo refrigeration circulator to temperatures below the freezing point of D_2O , $<4^\circ\text{C}$, into which the sample growth cell could be immersed in a controlled way by a stepper motor (Fig. 2), and the entire assembly was housed in a cold room at the Helmholtz-Zentrum Berlin (HZB) which was kept between 6°C and 10°C . The single crystal is selected from the polycrystalline ice, formed at the bottom of the growth cell, by continuous change in direction due to the lower part of the sample growth cell having a spiral form with a narrow sealed section at the lower end and a constriction at the upper end of the spiral. Ideally, one crystallite emerges from the spiral and continues to grow in a long, straight silicone-rubber tube with a 10-mm inner diameter. The heating gradient was enforced

by a circular heater placed around the growth cell about 3 cm above the ethylene glycol solution. Before growth, the starting D_2O in the cell was degassed by vacuum pumping and was sealed to prevent air contamination during growth, leading to a vapor pressure of approximately 30 mbar during growth. This growth method produced approximately 12-cm-long crystals over 1 week. The crystal was removed from the cell by cutting the rubber along its length and then cleaved perpendicular to its length into three pieces, one of which was used for the experiment. Crystal quality was tested using birefringence in the cold room or, when weather allowed, outside in the cold Berlin winter. The birefringence revealed the samples were composed of two twinned crystallites forming half cylinders along the entire length of the sample. One twin, a half cylinder 1 cm in diameter and 2 cm in length, was cleaved, and crystallinity was tested using x-ray Laue diffraction at a number of spots on all sides of the crystal, during which time the samples were orientated for the neutron measurements.

B. Neutron scattering

The structural correlations were measured on the E2 diffractometer at the BER-II reactor, Helmholtz-Zentrum Berlin, Germany [21], which uses a flat-cone geometry, and position-sensitive area detectors allow the measurement of the scattering intensity throughout volumes in 3D reciprocal space. Neutrons with a wavelength of 1.2 \AA were obtained using a [1,1,1] Ge monochromator with a 30-arcmin

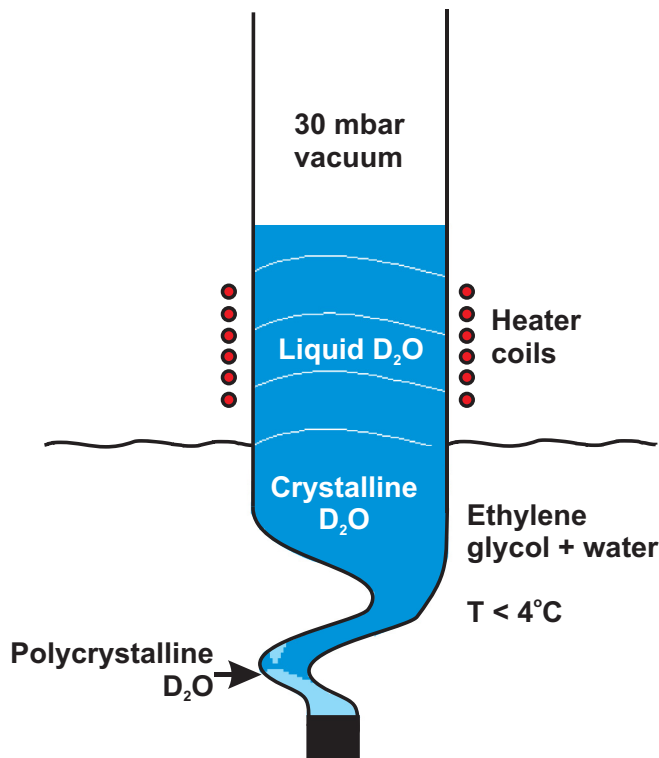


FIG. 2. Single-crystal growth cell based on work by Ohtomo *et al.* [20]. A rubber tube connected to a plastic spiral filled with D_2O is passed between heater coils and then lowered into a cooled ethylene glycol solution. Polycrystalline ice forms in the spiral, and directional changes select a single crystal which propagates into the main sample cell.

collimation. Data were collected by rotating the sample axis in steps of 1° , counting at each step for 1 min. The sample was oriented with the b - c plane in the horizontal scattering plane with data perpendicular to this plane being measured by synchronously tilting the detector bank and sample out of the scattering plane. Data were collected at 30 K using three different detector inclination angles between 0° and 30° . For the analysis, the data were transformed from angular space into three-dimensional reciprocal space using the orthorhombic unit cell [Fig. 1(a)] for Ih ice [22]. Lattice constants were checked with the E2 diffractometer at HZB and were found to be $a_{E2} = 4.30 \text{ \AA}$, $b_{E2} = 7.71 \text{ \AA}$, $c_{E2} = 7.27 \text{ \AA}$ on E2, agreeing with the literature [22] within the E2 instrument ω resolution of 1° . A closed-cycle refrigerator (CCR) kept the sample cold during measurements on E2, and the sample was transferred into the CCR under a cold N_2 atmosphere. To reduce background scattering the sample mount was covered with cadmium, and the CCR was operated without radiation shields. The lowest achievable temperature, and the temperature used in the neutron experiment, was 30 K.

III. DATA AND ANALYSIS

A. Three-dimensional fit to experimental data

The diffuse scattering between Bragg peaks shows broad features which reflect the hydrogen correlations. We analyze the 3D volume of neutron scattering data using a large-

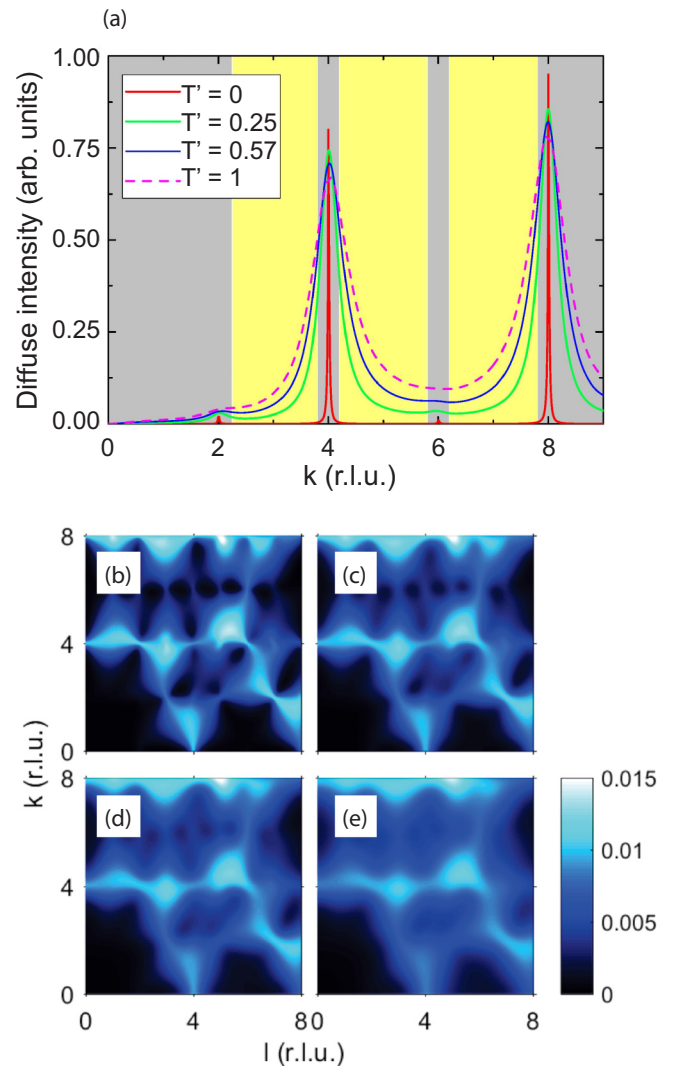


FIG. 3. Variation of theoretical diffuse scattering with respect to theoretical effective temperature T' . (a) The dependence of the theoretical diffuse scattering along $(0, k, 0)$ from hydrogen atoms on the value of the theoretical parameter T' from the large- N theory with $L = 16$ (L^3 is the number of units cells). At finite T' , the diffuse signal in the wings of the pinch points at $\vec{Q} = (0, 4, 0)$, and $(0, 8, 0)$ shows very distinct behavior as a function of Q . The yellow (light gray) regions represent the Q regions included in the fit to the experimental data showing a strong dependence on the calculated scattering with T' . Calculated neutron scattering intensity in the $(0, k, l)$ plane is shown for (b) $T' = 0.13J$, (c) $0.54J$, (d) $1.00J$, and (e) $2.00J$, revealing the dependence on T' of the diffuse scattering at and away from the pinch points. Therefore, a reliable value for T' can be obtained from the fit without including pinch points and areas around oxygen Bragg peaks [dark gray regions in (a)].

N approach [3]. Crucially, it captures both the short-range hydrogen correlations and the long-range distance decay in a unified analytical way. The actual analysis involves essentially standard diagonalization of the interaction matrix by the bonds of the oxygen network of ice, which is technically straightforward to carry out. Its nonstandard character, compared to conventional magnetic systems, lies in the nature of the solution thus obtained: the system avoids long-range

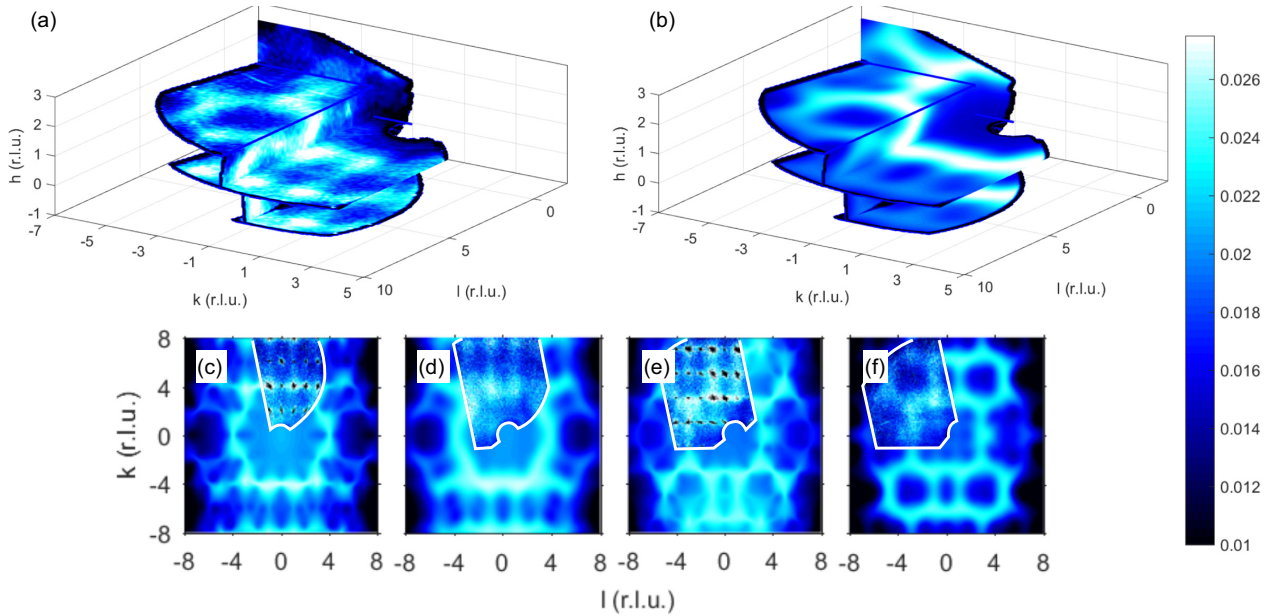


FIG. 4. Dipolar correlations in ice at 30 K. (a) A three-dimensional representation of the experimental neutron scattering data on noninteger indexed reciprocal space planes reveals diffuse textured features that come from the nontrivial hydrogen correlations. The data shown here are the $(h, k, -0.45)$, $(h, -0.45, l)$, $(h, -1.45, l)$, $(-0.45, k, l)$, $(0.55, k, l)$, and $(1.55, k, l)$ planes in reciprocal space. (b) The scattering calculated with the theory of Isakov *et al.* [3] using the parameters determined from the 3D fit to experimental data [Eq. (1) and Table I]. Further agreement between experiment and theory is shown on the (c) $(0, k, l)$, (d) $(0.5, k, l)$, (e) $(1.5, k, l)$, and (f) $(2.0, k, l)$ reciprocal lattice planes. The experimental neutron scattering data are shown inside the white lines, with black regions of the experimental data showing Bragg peaks and air scattering not included in the fit.

order down to the lowest temperatures and instead exhibits an extensive space of residual low-energy degrees of freedom. It is these which encode the emergent gauge structure.

The calculated intensity $I(Q)$ used in the fit is given by

$$I(Q) = I_0 G(Q, d, T') e^{(-BQ^2)} + a_0 + a_1|Q| + a_2|Q|^2. \quad (1)$$

Here I_0 is the incident neutron intensity per detector pixel in each $0.05 \times 0.05 \times 0.05$ reciprocal lattice unit (r.l.u.) Q -space volume element; $G(Q, d, T')$ is the theoretical structure factor, where d is the proton displacement away from the O-O bond midpoint and hence it is the length of the hydrogen displacement vector ($d = 0.134R_{OO}$) [3]. The Debye-Waller factor $e^{(-BQ^2)}$ accounts for the reduction in intensity due to atomic vibration; the remaining three terms account for the asymmetric background. The momentum transfer Q is the magnitude of the reciprocal lattice vector with coordinates (h, k, l) . The model contains only one free parameter resembling temperature in the effective interaction matrix (see Ref. [3]), T' , in units of the interaction strength J . The fit parameter T' characterizes the energy scale of the gauge theory J at finite temperature (Fig. 3) and is related to the energy scale for the first excited state; that is, T' sets the energy of the creation of ionic defect pairs in ice, H_3O^+ and OH^- [Fig. 1(d)], which are the analog to a monopole excitation in electromagnetism. The defect-defect correlation length ξ will increase proportionally with $e^{(+E/3k_B T')}$ (see Fig. 3), where E is the defect creation energy. Altogether, within the large- N model the constants d and T' fully describe the proton structure and a significant amount of the dynamics of ice within this gauge theory. The other parameters used in

the fit are related to the experimental setup. The experimental scattering data contains sharp Bragg peaks along with air scattering surrounding the intense Bragg peaks, neither of which is informative about the hydrogen correlations, so the fit function does not take those artifacts into account. Therefore, regions of Q space containing such scattering were excluded from the fit [Figs. 4(a) and 4(c)]. The fit is quite robust against the method of excluding such data points, with the effective interaction temperature always between $T' = 0.54J$ and $0.6J$ (Fig. 3), with the best-fit parameters given in Table I. The resulting diffuse neutron scattering data and calculation using the fit parameters are shown in Fig. 4, illustrating good agreement; the theory analytically fits the 3D diffuse scattering data from Ih ice.

TABLE I. The best-fit parameters from a simultaneous fit of the 3D experimental data at 30 K. Here “arb. units” represents arbitrary units, and “arb. units \AA ” and “arb. units \AA^2 ” refer to the same arbitrary units multiplied by angstroms and angstroms squared, respectively.

	Fit parameter	Standard error
a_0 (arb. units)	0.2699	0.0011
a_1 (arb. units \AA)	0.064	0.002
a_2 (arb. units \AA^2)	-0.066	0.002
T' (J)	0.57	0.08
I_0 (arb. units)	0.68	0.02
B (\AA^2)	0.161	0.08

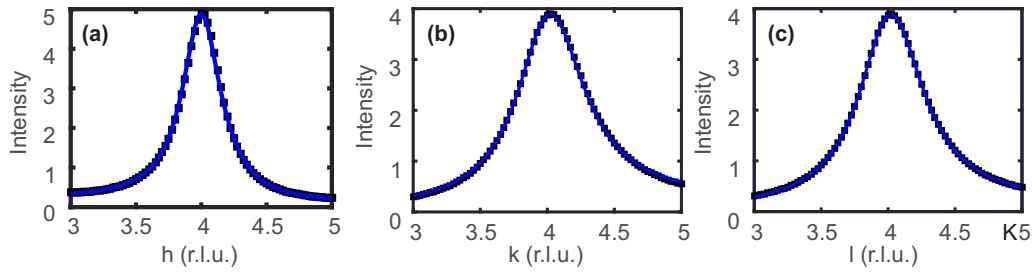


FIG. 5. Defect density at 30 K. To determine the defect correlation lengths the pinch points at the (a) (4,0,0), (b) (0,4,0), and (c) (0,0,4) positions in reciprocal space in the theoretical data (black squares) were fitted using an asymmetric background and Lorentzian line shapes (line).

B. Defect-defect correlation lengths, pinch points, and defect density

This analytic approach provides a method of probing ice properties that so far have not been accessible experimentally, namely, the determination of the defect density that is highly relevant, e.g., for electrical transport properties of ice. At sufficiently low temperatures, the ice rules are essentially almost perfectly obeyed, modulo the presence of dilute defects.

The experimental hydrogen correlations terminate at dilute point defects in the hydrogen structure, either ionic defects (OH^- , H_3O^+) or Bjerrum defects (either zero or two hydrogen ions between nearest-neighbor oxygen atoms, referred to as L and D defects, respectively [23]), or defects in the molecular structure (e.g., impurity ions, voids). In the ice literature, many properties are explained by the presence and mobility of such electrically charged defects [24,25]. Natural ice is usually impure, and partly for this reason a lot of studies have focused on doped ice, in particular for electrical transport properties. Within the ice literature a separation of the ionic and Bjerrum defect signals from impurities is therefore difficult.

In the diffuse scattering from matter described by gauge fields (e.g., water ice, spin ice) correlations are evident as broad features which narrow into a pinch point, resembling a bow tie, at specific locations in reciprocal space [3,17]. At finite temperature, the field lines, and therefore the hydrogen correlations in water ice, terminate at defects separated, on average, by the defect-defect correlation length, which experimentally is the inverse of the pinch-point width. In an ice crystal without defects, i.e., a crystal with only closed field lines, these pinch points would be perfectly sharp, and as defects are created, e.g., as temperature increases, the pinch points would be expected to broaden. The low-intensity pinch points and the intense Bragg peaks from the average structure unfortunately appear at the same positions in Q space in the experimental data, and in practice a reliable separation of these intensities at the pinch-point location is impossible. Since the experimental hydrogen correlations are quantitatively described by the theoretical fit to the experimental data, details of the pinch-point widths are nonetheless accessible in the neutron scattering intensity calculated using the parameters used to fit the experimental data [Eq. (1) and Table I]. In order to determine orthogonal correlation lengths, the (4,0,0), (0,4,0), and (0,0,4) pinch points in the theoretical data are fit with a Lorentzian function and an asymmetric background along the h , k , and l reciprocal space directions,

respectively [Figs. 5(a)–5(c)], using

$$I(q) = \frac{I_0^L \zeta^2}{\zeta^2 + (Q - Q_{hkl})^2} + I_{asym}. \quad (2)$$

The first term is the Lorentzian line shape, where I_0^L is the intensity at (h, k, l) ; ζ is the full width at half maximum of the Lorentzian at (h, k, l) measured in reciprocal lattice units and therefore related to the defect-defect correlation length ξ by $\zeta = 1/\xi$. Q is the magnitude of the reciprocal lattice vector; Q_{hkl} is the magnitude of the reciprocal lattice vector at the position of the (h, k, l) pinch point. The second term accounts for a low-intensity asymmetric background [Eq. (3)] with the asymmetry being needed to fit the wings of the theoretical data, although with little impact on the Lorentzian width due to the low asymmetry:

$$I_{asym}(q) = \frac{I_{b0}}{1 + e^{\frac{\pm Q - Q_{b0}}{\sigma}}} + I_{bc}, \quad (3)$$

where I_{b0} is the intensity at the center of the smoothed step function which is centered on Q_{b0} , \pm and \mp control whether the background has higher intensity at low Q or high Q , σ is the width of the step function, and I_{bc} is a constant background term. Other background functions, e.g., constant background and linear background, were used but did not fit the wings of the data well. The fit parameters are given in Table II; the three orthogonal defect-defect correlation lengths are approximately $9R_{\text{OO}}$, resulting in a defect density of one defect per 500 sites.

IV. DISCUSSION AND CONCLUSION

The experimental and theoretical methods shown here are promising tools to get more insight into the physics of ice. In principle the structure factor of the different defects could be used to distinguish between ionic and Bjerrum defects, but the Q -space range here and current data statistics preclude such an identification. Nevertheless, the technique reported here allows for a reliable determination of the density of the *total* number of defects. It is of interest to note that within the model, hopping of a hydrogen from one site along the OH-O bond to another site is described as reversal of the emergent field between a neighboring oxygen-oxygen pair, resulting in the flipping of an individual pseudospin, creating a pair of emergent gauge charges. As the pseudospins also correlated with electric dipole moments on bonds (note that the molecular electric dipole moment would be the sum of the

TABLE II. Fit parameters of the (4,0,0), (0,4,0), and (0,0,4) pinch points in the large- N theoretical fit to the experimental data [Figs. 5(a)–5(c)], where au indicates arbitrary units.

	ζ (r.l.u.)	ξ	I_{bc} (au)	I_{b0} (au)	σ (r.l.u.)	q_{b0} (r.l.u.)
($h, 0, 0$)	0.1766	$5.663a = 25.5 \text{ \AA}$	7.6339	12.04	0.0464	4.35
($0, k, 0$)	0.3138	$3.186b = 24.9 \text{ \AA}$	2.7×10^{-4}	25.23	0.0574	3.855
($0, 0, l$)	0.2985	$3.351c = 24.7 \text{ \AA}$	2.7×10^{-4}	16.76	0.057	3.85

pseudospins coming into a particular oxygen), the resulting excitations in the theory also carry conventional electric charge and can be thought of (roughly) as plus (H_3O^+) and minus (OH^-) defects [Fig. 1(d)]. The ionic defects, once created, are mobile through the reversal of neighboring pseudospins (i.e., neighboring protons moving between occupied and vacant sites), leading to molecular rotation along the path traveled by the ionic defect, retaining some of the structural mutability of the liquid phase and accounting, in part, for ice's electrical conductivity [1,26,27]. It is important to note that the flipping of pseudospins to account for electrical conductivity is not in the quantum tunneling regime as predicted by Benton *et al.* [16], which occurs at much lower temperatures than were probed in this study.

The correlation length estimate here reveals an average defect density of one defect per 500 oxygen sites, corresponding to $1.2 \times 10^{21} \text{ mol}^{-1}$ in our sample at 30 K. That may be compared to previous high-temperature work in which a *higher* concentration would be expected: Gränicher reported that the defect densities at 263 K are $1.6 \times 10^{12} \text{ mol}^{-1}$ for ionic defects and $1.1 \times 10^{17} \text{ mol}^{-1}$ for Bjerrum defects [25]. Khamzin and Nigmatullin [28], when using a model of electrical relaxation due to ion hopping [29], showed that Gränicher's defect densities are not sufficient to account for the experimentally observed dielectric strengths at 200 and 250 K [30]. Indeed, a defect density of $5.9 \times 10^{22} \text{ mol}^{-1}$, approximately 50 times the density we found in our sample at 30 K, would be needed at 200 and 250 K to account for the dielectric strengths. Further temperature-dependent measurements of the defect density, such as ours, and of the dielectric constant would be instructive and shed more light on this problem, but they are beyond the scope of the present study.

In summary, using neutron diffraction we showed that the highly degenerate low-temperature structure of Ih ice is described by an analytical theory mapping ice-rule constrained hydrogen displacements onto an emergent electromagnetic field with U(1) symmetry. The hydrogen correlations follow

its field lines, and the field, mostly divergence free, locally contains dilute point defects in the hydrogen correlations corresponding to weakly interacting gauge charges. These charges terminate the field lines and therefore degrade the hydrogen correlations. The success of the theory in fitting ice data is of general importance as it provides another tool in the analysis of diffuse scattering data which probes the nano- and mesoscale disorder which in many functional materials underpins their sensitivity to external stimuli [31]. The usefulness of this technique is exemplified by the determination of the density of intrinsic point defects which play an important role in the response of Ih ice to stimuli such as applied fields, with these defects being found to be present at one defect per 500 sites at 30 K in our sample. Whether cooperative effects of these point defects become more important to structural correlations or dynamics, e.g., as their density and quantum coherence vary with temperature, is an intriguing question which now is open to investigation.

Data sets containing neutron diffraction data and theoretical calculated data are available in Ref. [32].

ACKNOWLEDGMENTS

We wish to thank T. Hauß, A. Hoser, and K. Kiefer (HZB) for assistance with the experiment; B. Lake and E. Weschke (HZB) for manuscript proof-reading; and O. Benton (Okinawa Institute of Science and Technology), I. A. Ryzhkin (Institute of Solid State Physics), and D. T. W. Buckingham (Montana State University) for scientific discussions. We acknowledge financial support provided by the Helmholtz Association of German Research Centers as well as Deutsche Forschungsgemeinschaft under Grants No. SFB 1143 and No. EXC 2147 ct.qmat. The research by D.A.T. was sponsored by the Laboratory Directed Research and Development Program (LDRD) of Oak Ridge National Laboratory, managed by UT-Battelle, LLC, for the U.S. Department of Energy (Project ID 9566).

[1] L. Onsager, in *Nobel Lectures, Chemistry 1963–1970* (Elsevier, Amsterdam, 1972), pp. 272–288.
[2] P. V. Hobbs, *Ice Physics* (Oxford University Press, Oxford, 1974).
[3] S. V. Isakov, R. Moessner, S. L. Sondhi, and D. A. Tennant, *Phys. Rev. B* **91**, 245152 (2015).
[4] J. D. Bernal and R. H. Fowler, *J. Chem. Phys.* **1**, 515 (1933).
[5] L. Pauling, *J. Am. Chem. Soc.* **57**, 2680 (1935).
[6] J. Schneider and C. Zeyen, *J. Phys. C* **13**, 4121 (1980).

[7] V. M. Nield, J. C. Li, D. K. Ross, and R. W. Whitworth, *Phys. Scripta* **T57**, 179 (1995).
[8] B. Wehinger, D. Chernyshov, M. Krisch, S. Bulat, V. Ezhov, and A. Bosak, *J. Phys.: Condens. Matter* **26**, 265401 (2014).
[9] J. Villain, *Solid State Commun.* **10**, 967 (1972).
[10] J. F. Nagle, *Chem. Phys.* **43**, 317 (1979).
[11] R. Youngblood, J. D. Axe, and B. M. McCoy, *Phys. Rev. B* **21**, 5212 (1980).
[12] R. W. Youngblood and J. D. Axe, *Phys. Rev. B* **23**, 232 (1981).

- [13] I. Ryzhkin, *Solid State Commun.* **52**, 49 (1984).
- [14] I. A. Ryzhkin, *J. Exp. Theor. Phys.* **88**, 1208 (1999).
- [15] A. H. Castro Neto, P. Pujol, and E. Fradkin, *Phys. Rev. B* **74**, 024302 (2006).
- [16] O. Benton, O. Sikora, and N. Shannon, *Phys. Rev. B* **93**, 125143 (2016).
- [17] C. L. Henley, *Annu. Rev. Condens. Matter Phys.* **1**, 179 (2010).
- [18] C. Castelnovo, R. Moessner, and S. L. Sondhi, *Annu. Rev. Condens. Matter Phys.* **3**, 35 (2012).
- [19] V. F. Sears, *Neutron News* **3**, 26 (1992).
- [20] M. Ohtomo, S. Ahmad, and R. W. Whitworth, *J. Phys. Colloques* **48**, C1-595 (1987).
- [21] J.-U. Hoffmann and M. Reehuis, *J. Large Scale Res. Facil.* **4**, A129 (2018).
- [22] J. A. Hayward and J. R. Reimers, *J. Chem. Phys.* **106**, 1518 (1997).
- [23] N. Bjerrum, *Science* **115**, 385 (1952).
- [24] H. Engelhardt, B. Bullemer, and N. Riehl, in *Physics of Ice*, (Plenum, New York, 1969), pp. 430–442.
- [25] H. Gränicher, *Phys. Kondens. Mater.* **1**, 1 (1963).
- [26] C. A. Coulson and D. Eisenberg, *Proc. R. Soc. London, Ser. A* **291**, 445 (1966).
- [27] C.-W. Lee, P.-R. Lee, Y.-K. Kim, and H. Kang, *J. Chem. Phys.* **127**, 084701 (2007).
- [28] A. A. Khamzin and R. R. Nigmatullin, *J. Chem. Phys.* **147**, 204502 (2017).
- [29] D. L. Sidebottom, *Rev. Mod. Phys.* **81**, 999 (2009).
- [30] S. Kawada, *J. Phys. Soc. Jpn.* **44**, 1881 (1978).
- [31] D. A. Keen and A. L. Goodwin, *Nature (London)* **521**, 303 (2015).
- [32] J.-U. Hoffmann, K. Siemensmeyer, S. Isakov, D. J. P. Morris, B. Klemke, I. Glavatskyi, K. Seiffert, D. A. Tennant, S. Sondhi, and R. Moessner, Neutron study of the topological flux model of hydrogen ions in water ice (2018), <http://dx.doi.org/10.5442/ND000001>.